Nonlinear Backstepping Control for Three-Phase Single-Stage Grid-Tied Photovoltaic Systems via an LCL-Filter

Zakariae El Madani
Computer Engineering and Intelligent Electrical Systems Laboratory, EST, Moulay Ismail University, Meknes, Morocco
zakariae.elmadani@gmail.com (corresponding author)

Abdelhafid Yahya
Computer Engineering and Intelligent Electrical Systems Laboratory, EST, Moulay Ismail University, Meknes, Morocco
yaabha2@gmail.com

Zakaria El Malki
Computer Engineering and Intelligent Electrical Systems Laboratory, EST, Moulay Ismail University, Meknes, Morocco
zelmalki@yahoo.fr

Received: 14 August 2024 | Revised: 16 September 2024 | Accepted: 27 September 2024

 DOI: https://doi.org/10.48084/etasr.8722

ABSTRACT

This paper examines the modeling and nonlinear control of a Three-Phase Single-Stage Grid-Tied Photovoltaic System (TPSS-GTPS). The system structure is relatively simple, comprising a Photovoltaic (PV) generator connected to the grid through a three-phase Voltage Source Inverter (VSI) and an LCL filter designed to reduce harmonics in the grid current. The primary objective of the control system is to maximize the extraction of power from the Photovoltaic Generator (PVG) and deliver it to the utility grid with a Unity Power Factor (UPF), while ensuring the asymptotic stability of the closed-loop system. In order to achieve these objectives, a novel nonlinear controller was developed in the synchronous dq-frame following the backstepping approach. Evaluating the effectiveness of the designed controller, simulations were performed in the MATLAB/Simulink environment under various scenarios to consider the effects of irradiance and temperature on the PVG. The simulation results demonstrated that the controller successfully achieved all the specified objectives. Additionally, this study highlights the effectiveness of the LCL filter in reducing Total Harmonic Distortion (THD).

Keywords-PV system; single-stage; LCL-filter; nonlinear backstepping control; Maximum Power Point Tracking (MPPT); Unity Power Factor (UPF)

I. INTRODUCTION

In recent years, the power generation sector has seen a notable integration of renewable energy sources, including solar, wind, and others. In particular, PV solar energy has become a popular type of renewable energy source for a variety of reasons, including its capacity to produce clean, sustainable energy with a minimal environmental impact. Moreover, PV systems are distinguished by their simplicity of installation and maintenance, rendering them well-suited for a multitude of applications [1].

The power generated by PVGs can be used in two primary applications: first, in standalone PV systems [2, 3] that rely on energy storage in a battery bank and are typically employed for low-power requirements, such as in residential settings, and second, in grid-tied PV systems [4-7] that supply power directly to the grid while maintaining a nearly unity power factor despite environmental fluctuations. In order to maximize the effectiveness of PV systems, it is essential to operate the generators at their Maximum Power Point (MPP). This can be achieved through the use of Maximum Power Point Tracking (MPPT) techniques. A review of the literature reveals the existence of numerous MPPT control algorithms [8-13], with the Perturbation and Observation (PO) and Incremental Conductance (IC) techniques being the most extensively examined ones. In grid-tied PV applications, the power by PV generators can be integrated into the utility grid through the use

of power converters. In general, there are two principal configurations, as outlined in [14]. The first configuration is the double-stage PV system [15, 16], wherein the PV generators are connected to the grid through a DC/DC boost converter for MPPT, and a VSI for Power Factor Correction (PFC). The second configuration, defined as the single-stage PV system, connects the PV generators directly to the electricity grid via a DC/AC converter that performs both MPPT and PFC functions [5, 17, 18]. The single-stage configuration is frequently the preferred option due to its efficiency in optimizing the energy conversion process, simplifying circuit design, reducing the overall system size, and lowering costs. A conventional VSI is responsible for managing energy conversion and injecting the sinusoidal current into the grid. In order to enhance the quality of the injected current, a number of filters have been examined in the literature, including L, LC, and LCL filters [17–22]. Among these, the LCL filter is particularly favored for its superior performance, offering better attenuation, smaller inductor sizes, and the ability to operate at lower switching frequencies.

A plethora of control strategies for TPSSs with LCL filters have been presented, with a particular emphasis on both MPPT and achieving a UPF. Authors in [23] put forth a two-loop control strategy that employs a conventional PI controller, whereas authors in [24] presented a two-loop control scheme that incorporates a PR resonant controller. Authors in [25] proposed a hybrid controller combining the state feedback pole-assignment control with repetitive control. Furthermore, authors in [26] introduced a simplified feedback linearization control strategy. An adaptive control scheme is outlined by authors in [27], while authors in [28] presented an output feedback model reference adaptive control scheme.

The primary contributions of this research were:

- A mathematical model was developed in the synchronous dq-frame for a TPSS-GTPS with an LCL filter.
- A novel nonlinear controller based on the backstepping approach is proposed to achieve multiple objectives, including the MPPT and UPF on the grid side, while ensuring the asymptotic stability of the closed-loop system.
- The power quality delivered to the electricity grid is enhanced by reducing the THD through the utilization of an LCL filter.

This paper begins its research with the modeling and configuration of the power system and continues with a detailed account of the proposed control approach. Furthermore, it presents and evaluates the simulation results, leading to the conclusions.

II. POWER SYSTEM DESCRIPTION AND MODELING

A. Photovoltaic Generator Configuration

In this study, a PVG comprising sixteen parallel strings, with each string containing thirty-four modules connected in series, was employed. Table I shows the specific parameters of the used PV modules. Figure 1 presents the power-voltage characteristic curves of the generator under varying levels of solar irradiation and temperature. Table II demonstrates the corresponding maximum power output at these conditions. This table will be used during the simulation phase to validate the MPPT.

TABLE I. NU-183E1 CHARACTERISTICS UNDER STC

Parameter	Symbol	Value
Number of series cells	N_s	48
Number of parallel cells	N_p	1
Maximum power	P_{max}	183 W
Voltage at MPP	V_{mpp}	23.9 V
Current at MPP	I_{mpp}	7.66 A
Short circuit current	I_{sc}	8.48 A
Open circuit voltage	V_{oc}	30.1 V

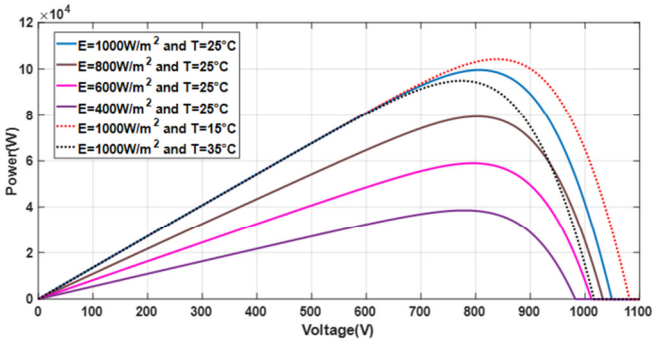

Fig. 1. Power-voltage characteristic curves of the PVG under different levels of solar irradiation and temperature.

TABLE II. MAXIMUM POWER OUTPUT AT DIFFERENT LEVELS OF IRRADIATION AND TEMPERATURE

Irradiation (W/ m^2)	Temperature (°C)	MPP (kW)
400	25	38.515
600	25	58.979
800	25	79.395
1,000	25	99.608
1,000	35	94.954
1,000	15	104.279

B. Power System Modeling

Figure 2 depicts the PV system that is the subject of this study. The power circuit comprises four principal components: a PVG, a three-phase voltage source inverter, an LCL filter, and a three-phase grid. The inverter circuit is comprised of three legs, each of which contains two semiconductor switches that are controlled by Pulse Width Modulation (PWM) signals, S_a, S_b and S_c, which attain values within the set {0,1}. The LCL filter comprises an inductance (L_i) on the inverter side, a capacitor, and an inductance (L_g) on the grid side, along with the corresponding equivalent resistances (R_i) and (R_g), respectively. In this context, the notations i_i, u_c, and i_g are employed to represent the inverter-side current, filter capacitor voltage, and grid-side current, respectively. The grid inductance is incorporated into the grid-side filter inductance, and it is assumed that the grid voltages e_{ga}, e_{gb}, and e_{gc} constitute a balanced three-phase system.

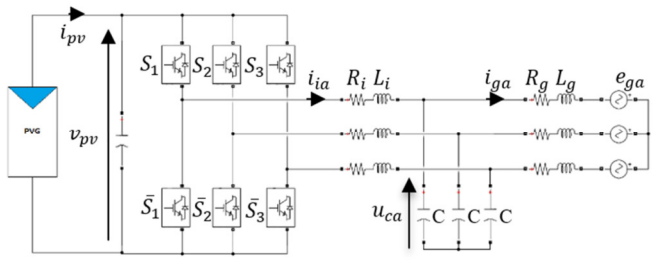

Fig. 2. Topology of the three-phase single-stage grid-tied PV system.

By applying Kirchhoff's laws to the circuit, the following switching model is derived in the abc-frame:

$$L_g.\frac{d}{dt}\begin{bmatrix} i_{ga} \\ i_{gb} \\ i_{gc} \end{bmatrix} = -R_g \begin{bmatrix} i_{ga} \\ i_{gb} \\ i_{gc} \end{bmatrix} + \begin{bmatrix} u_{ca} \\ u_{cb} \\ u_{cc} \end{bmatrix} - \begin{bmatrix} e_{ga} \\ e_{gb} \\ e_{gc} \end{bmatrix} \quad (1)$$

$$C.\frac{d}{dt}\begin{bmatrix} u_{ca} \\ u_{cb} \\ u_{cc} \end{bmatrix} = \begin{bmatrix} i_{ia} \\ i_{ib} \\ i_{ic} \end{bmatrix} - \begin{bmatrix} i_{ga} \\ i_{gb} \\ i_{gc} \end{bmatrix} \quad (2)$$

$$L_i.\frac{d}{dt}\begin{bmatrix} i_{ia} \\ i_{ib} \\ i_{ic} \end{bmatrix} = -R_f \begin{bmatrix} i_{ia} \\ i_{ib} \\ i_{ic} \end{bmatrix} + \frac{v_{pv}}{3}\begin{bmatrix} 2 & -1 & -1 \\ -1 & 2 & -1 \\ -1 & -1 & 2 \end{bmatrix}\begin{bmatrix} S_1 \\ S_2 \\ S_3 \end{bmatrix} - \begin{bmatrix} u_{ca} \\ u_{cb} \\ u_{cc} \end{bmatrix} \quad (3)$$

$$C_{pv}.\frac{dv_{pv}}{dt} = i_{pv} - [S_1 \quad S_2 \quad S_3]\begin{bmatrix} i_{ia} \\ i_{ib} \\ i_{ic} \end{bmatrix} \quad (4)$$

where S_1, S_2, and S_3 are the control input signals, taking values from the finite set {0, 1}.

The character of the control input signals is such that the previously described model, which was based on switching, is no longer appropriate for the design of a regulator. In order to address this issue and facilitate the design of a regulator for the system under study, the use of the following averaged model, which is obtained by (1) – (4) over the switching period T_s [29], is proposed:

$$L_g.\frac{d}{dt}\begin{bmatrix} I_{ga} \\ I_{gb} \\ I_{gc} \end{bmatrix} = -R_g \begin{bmatrix} I_{ga} \\ I_{gb} \\ I_{gc} \end{bmatrix} + \begin{bmatrix} U_{ca} \\ U_{cb} \\ U_{cc} \end{bmatrix} - \begin{bmatrix} E_{ga} \\ E_{gb} \\ E_{gc} \end{bmatrix} \quad (5)$$

$$C.\frac{d}{dt}\begin{bmatrix} U_{ca} \\ U_{cb} \\ U_{cc} \end{bmatrix} = \begin{bmatrix} I_{ia} \\ I_{ib} \\ I_{ic} \end{bmatrix} - \begin{bmatrix} I_{ga} \\ I_{gb} \\ I_{gc} \end{bmatrix} \quad (6)$$

$$L_i.\frac{d}{dt}\begin{bmatrix} I_{ia} \\ I_{ib} \\ I_{ic} \end{bmatrix} = -R_i \begin{bmatrix} I_{ia} \\ I_{ib} \\ I_{ic} \end{bmatrix} + \frac{V_{pv}}{3}\begin{bmatrix} 2 & -1 & -1 \\ -1 & 2 & -1 \\ -1 & -1 & 2 \end{bmatrix}\begin{bmatrix} \mu_a \\ \mu_b \\ \mu_c \end{bmatrix} - \begin{bmatrix} U_{ca} \\ U_{cb} \\ U_{cc} \end{bmatrix} \quad (7)$$

$$C_{pv}.\frac{dV_{pv}}{dt} = I_{pv} - [\mu_a \quad \mu_b \quad \mu_c]\begin{bmatrix} I_{ia} \\ I_{ib} \\ I_{ic} \end{bmatrix} \quad (8)$$

where $I_{ia,b,c}$, $I_{ga,b,c}$, $U_{ca,b,c}$, V_{pv}, and $\mu_{a,b,c}$ represent the average values over the switching period T_s of the signals $i_{ia,b,c}$, $i_{ga,b,c}$, $u_{ca,b,c}$, v_{pv}, and $s_{1,2,3}$, respectively. The averaged model in the abc-frame, represented by (5)-(8), is a time-variant and nonlinear function. In order to render it time-invariant, Park's transformation is applied and the model of the complete system in the synchronous dq-frame is obtained as:

$$L_g.\dot{I}_{gd} = L_g.\omega.I_{gq} - R_g.I_{gd} + U_{cd} - E_{gd} \quad (9)$$

$$L_g.\dot{I}_{gq} = -L_g.\omega.I_{gd} - R_g.I_{gq} + U_{cq} - E_{gq} \quad (10)$$

$$C.\dot{U}_{cd} = C.\omega.U_{cq} + I_{id} - I_{gd} \quad (11)$$

$$C.\dot{U}_{cq} = -C.\omega.U_{cd} + I_{iq} - I_{gq} \quad (12)$$

$$L_i.\dot{I}_{id} = L_i.\omega.I_{iq} - R_i.I_{id} + V_{pv}.\mu_d - U_{cd} \quad (13)$$

$$L_i.\dot{I}_{iq} = -L_i.\omega.I_{id} - R_i.I_{iq} + V_{pv}.\mu_q - U_{cq} \quad (14)$$

$$C_{pv}.\dot{V}_{pv} = I_{pv} - \frac{3}{2}(\mu_d.I_{id} + \mu_q.I_{iq}) \quad (15)$$

Equations (9)-(15) represent the complete dynamical model of a TPSS GTPS. This model is time-invariant and nonlinear due to the to the presence of terms $v_{pv}.\mu_d$, $v_{pv}.\mu_q$, $\mu_d.i_{id}$, and $\mu_q.i_{iq}$. In the synchronous dq-frame, the active and reactive power supplied to the grid can be written as [30]:

$$P_g = \frac{3}{2}(E_{gd}.I_{gd} + E_{gq}.I_{gq}) \quad (16)$$

$$Q_g = \frac{3}{2}(E_{gq}I_{gd} - E_{gd}I_{gq}) \quad (17)$$

where E_{gd} and E_{gq} are the d-axis and q-axis voltage components of the grid, respectively, and I_{gd}, I_{gd} are the d-axis and q-axis current components of the grid. According to (16) and (17), both P and Q depend on both the d-axis and q-axis quantities, making independent control of P and Q complex. Let us assume that the grid voltage component E_{gq} is set to zero. In this case, the active power P and the reactive power Q can be expressed as:

$$P_g = \frac{3}{2}E_{gd}.I_{gd} \quad (18)$$

$$Q_g = -\frac{3}{2}E_{gd}I_{gq} \quad (19)$$

III. CONTROL SYSTEM DEVELOPMENT

This section presents a detailed analysis and design of a nonlinear backstepping controller for a TPSS-GTPS system equipped with an LCL filter. The principal objectives of the controller are to guarantee operation at the MPP, maintain a UPF on the grid, and ensure the closed-loop system's overall asymptotic stability, irrespective of the varying atmospheric conditions. In order to achieve a UPF on the grid (i.e. zero reactive power), it is necessary for the control law to ensure that the grid current I_q is regulated to match the reference current I^*_{gq}=0. Furthermore, the control law must also ensure that the PV power P_{pv} follows the desired PV power P^*_{pv} in order to maintain the system operating at the MPP. The reference power P^*_{pv} is generated using the PO method. Under the assumption that the inverter is lossless and that the power loss in the LCL filter is negligible, the power generated by the

PVG is equal to the active power delivered to the grid. Therefore:

$$P_g = \frac{3}{2} E_{gd}.I_{gd} = P_{pv} \quad (20)$$

Assuming that both objectives, the MPPT and UPF on the grid side, are effectively satisfied, from the above equations, it can be obtained:

$$I_{gd}^* = \frac{2P_{pv}^*}{3E_{gd}} \text{ and } I_{gq}^* = 0 \quad (21)$$

A. Design of a Nonlinear Backstepping Controller

This section aims to derive the control laws, μ_d and μ_q, to ensure that the LCL filter's output currents, I_{gd} and I_{gq}, track their reference values, I_{gd}^* and I_{gq}^*. This will certify the simultaneous achievement of the key objectives: operating at the MPP and maintaining a UPF on the grid. To achieve these goals, a control strategy based on the backstepping approach is used:

- Step 1: Stabilization of (9) and (10):

These are the tracking errors:

$$z_1 = L_g(I_{gd} - I_{gd}^*) \quad (22)$$

$$z_2 = L_g(I_{gq} - I_{gq}^*) \quad (23)$$

The time derivatives of z_1 and z_2 are:

$$\dot{z}_1 = L_g(\dot{I}_{gd} - \dot{I}_{gd}^*) \quad (24)$$

$$\dot{z}_2 = L_g(\dot{I}_{gq} - \dot{I}_{gq}^*) \quad (25)$$

By substituting the values of $\dot{I}_{gd}$ from (9) and $\dot{I}_{gq}$ from (10), $\dot{z}_1$ and $\dot{z}_2$ can be described as:

$$\dot{z}_1 = L_g.\omega.I_{gq} - R_g.I_{gd} + U_{cd} - E_{gd} - L_g\dot{I}_{gd}^* \quad (26)$$

$$\dot{z}_2 = -L_g.\omega.I_{gd} - R_g.I_{gq} + U_{cq} - E_{gq} - L_g\dot{I}_{gq}^* \quad (27)$$

Then, by considering the Lyapunov candidate function V_1:

$$V_1 = \frac{1}{2}z_1^2 + \frac{1}{2}z_2^2 \quad (28)$$

The time derivative of V_1 is:

$$\dot{V}_1 = z_1\dot{z}_1 + z_2\dot{z}_2 \quad (29)$$

By substituting $\dot{z}_1$ from (26) and $\dot{z}_2$ from (27), the expression for $\dot{V}_1$ is given by:

$$\dot{V}_1 = z_1.(L_g.\omega.I_{gq} - R_g.I_{gd} + U_{cd} - E_{gd} - L_g\dot{I}_{gd}^*) + z_2.(-L_g.\omega.I_{gd} - R_g.I_{gq} + U_{cq} - E_{gq} - L_g\dot{I}_{gq}^*) \quad (30)$$

The system will achieve asymptotic stability if $\dot{V}_1 \leq 0$. By choosing U_{cd} and U_{cq} as virtual control inputs, the following stabilizing functions are obtained:

$$U_{cd} = \alpha_1 = -c_1.z_1 - L_g.\omega.I_{gq} + R_g.I_{gd} + E_{gd} + L_g\dot{I}_{gd}^* \quad (31)$$

$$U_{cq} = \alpha_2 = -c_2.z_2 + L_g.\omega.I_{gd} + R_g.I_{gq} + E_{gq} + L_g\dot{I}_{gq}^* \quad (32)$$

where c_1 and c_2 are positive constant parameters, which are used to adjust the output responses of the system. In fact, this choice leads to:

$$\dot{V}_1 = -c_1.z_1^2 - c_2.z_2^2 \leq 0 \quad (33)$$

Since U_{cd} and U_{cq} are not the actual control inputs, the new error variables, z_3 and z_4, are introduced:

$$z_3 = C(U_{cd} - \alpha_1) \quad (34)$$

$$z_4 = C(U_{cq} - \alpha_2) \quad (35)$$

By using (26), (27), (31), (32), (34), and (35), the time derivatives of z_1, z_2, and V_1 become:

$$\dot{z}_1 = -c_1.z_1 + \frac{z_3}{C} \quad (36)$$

$$\dot{z}_2 = -c_2.z_2 + \frac{z_4}{C} \quad (37)$$

$$\dot{V}_1 = -c_1.z_1^2 - c_2.z_2^2 + \frac{z_1.z_3}{C} + \frac{z_2.z_4}{C} \quad (38)$$

- Step 2: Stabilization of (11) and (12):

Using the same method as the previous step and (11) and (12), the time derivatives of z_3 and z_4 are:

$$\dot{z}_3 = C.\omega.U_{cq} + I_{id} - I_{gd} - C.\dot{\alpha}_1 \quad (39)$$

$$\dot{z}_4 = -C.\omega.U_{cd} + I_{iq} - I_{gq} - C.\dot{\alpha}_2 \quad (40)$$

Then, by defining the augmented Lyapunov candidate function V_2:

$$V_2 = V_1 + \frac{1}{2}z_3^2 + \frac{1}{2}z_4^2 \quad (41)$$

Using (38), the dynamic of V_2 gives:

$$\dot{V}_2 = -c_1.z_1^2 - c_2.z_2^2 + z_3.\left(\frac{z_1}{C} + \dot{z}_3\right) + z_4.(\frac{z_2}{C} + \dot{z}_4) \quad (42)$$

By substituting the values of $\dot{z}_3$ from (39) and $\dot{z}_4$ from (40), $\dot{V}_2$ becomes:

$$\dot{V}_2 = -c_1z_1^2 + z_3.(\frac{z_1}{C} + C.\omega.U_{cq} + I_{id} - I_{gd} - C\dot{\alpha}_1) - c_2.z_2^2 + z_4.(\frac{z_2}{C} - C.\omega.U_{cd} + I_{iq} - I_{gq} - C\dot{\alpha}_2) \quad (43)$$

The system is asymptotically stable if $\dot{V}_2 \leq 0$. The following stabilizing functions are obtained by choosing I_{id} and I_{iq} as virtual control inputs:

$$I_{id} = \alpha_3 = -c_3.z_3 - \frac{z_1}{C} - C.\omega.U_{cq} + I_{gd} + C.\dot{\alpha}_1 \quad (44)$$

$$I_{iq} = \alpha_4 = -c_4.z_4 - \frac{z_2}{C} + C.\omega.U_{cd} + I_{gq} + C.\dot{\alpha}_2 \quad (45)$$

where c_3 and c_4 are positive constant parameters. Indeed, this choice implies that:

$$\dot{V}_2 = -c_1.z_1^2 - c_2.z_2^2 - c_2.z_2^2 - c_4.z_4^2 \leq 0 \quad (46)$$

As I_{id} and I_{iq} are not the actual control inputs, the new error variables, z_5 and z_6, are defined:

$$z_5 = L_i(I_{id} - \alpha_3) \quad (47)$$

$$z_6 = L_i(I_{iq} - \alpha_4) \quad (48)$$

By using (39), (40), (44), (45), (47), and (48), $\dot{z}_3$, $\dot{z}_4$, and $\dot{V}_2$ become:

$$\dot{z}_3 = -c_3.z_3 - \frac{z_1}{C} + \frac{z_5}{L_i} \quad (49)$$

$$\dot{z}_4 = -c_4.z_4 - \frac{z_2}{C} + \frac{z_6}{L_i} \quad (50)$$

$$\dot{V}_2 = -c_1.z_1^2 - c_2.z_2^2 - c_3.z_3^2 - c_4.z_4^2 + \frac{z_3 z_5}{L_i} + \frac{z_4 z_6}{L_i} \quad (51)$$

- Step3: Stabilizing of (13) and (14)

Utilizing (13) and (14), the time derivatives of z_5 and z_6 can be expressed as:

$$\dot{z}_5 = L_i.\omega.I_{iq} - R_i.I_{id} + V_{pv}.\mu_d - U_{cd} - L_i\dot{\alpha}_3 \quad (52)$$

$$\dot{z}_6 = -L_i.\omega.I_{id} - R_i.I_{iq} + V_{pv}.\mu_q - U_{cq} - L_i.\dot{\alpha}_4 \quad (53)$$

Then, defining the augmented Lyapunov candidate function V_3, gives:

$$V_3 = V_2 + \frac{1}{2}z_5^2 + \frac{1}{2}z_6^2 \quad (54)$$

Using (51), the dynamic of the Lyapunov candidate function V_3 gives:

$$\dot{V}_3 = -c_1.z_1^2 - c_2.z_2^2 - c_3.z_3^2 - c_4.z_4^2 + z_5.(\frac{z_3}{L_i} + \dot{z}_5) + z_6.(\frac{z_4}{L_i} + \dot{z}_6) \quad (55)$$

For making V_3 a negative definite function, let us take:

$$\dot{z}_5 = -c_5.z_5 - \frac{z_3}{L_i} \quad (56)$$

$$\dot{z}_6 = -c_6.z_6 - \frac{z_4}{L_i} \quad (57)$$

where c_5 and c_6 are positive constant parameters. Indeed, this choice implies that:

$$\dot{V}_3 = -c_1.z_1^2 - c_2.z_2^2 - c_2.z_2^2 - c_4.z_4^2 - c_5.z_5^2 - c_6.z_6^2 \leq 0 \quad (58)$$

By comparing (52) with (56) and (53) with (57), the control laws can be derived:

$$\mu_d = \frac{1}{V_{pv}}(-c_5.z_5 - \frac{z_3}{L_i} - L_i.\omega.I_{iq} + R_i.I_{id} + U_{cd} + L_i\dot{\alpha}_3) \quad (59)$$

$$\mu_q = \frac{1}{V_{pv}}(-c_6.z_6 - \frac{z_4}{L_i} + L_i.\omega.I_{id} + R_i.I_{iq} + U_{cq} + L_i.\dot{\alpha}_4) \quad (60)$$

Consider the system defined by the state-space equations (9)-(14) and the control laws (59)-(60). In closed-loop, the system behavior in the error coordinates $(z_1, z_2, z_3, z_4, z_5, z_6)$ is given by:

$$\begin{bmatrix} \dot{z}_1 \\ \dot{z}_2 \\ \dot{z}_3 \\ \dot{z}_4 \\ \dot{z}_5 \\ \dot{z}_6 \end{bmatrix} = \begin{bmatrix} -c_1 & 0 & \frac{1}{C} & 0 & 0 & 0 \\ 0 & -c_2 & 0 & \frac{1}{C} & 0 & 0 \\ -\frac{1}{C} & 0 & -c_3 & 0 & \frac{1}{L_i} & 0 \\ 0 & -\frac{1}{C} & 0 & -c_4 & 0 & \frac{1}{L_i} \\ 0 & 0 & -\frac{1}{L_i} & 0 & -c_5 & 0 \\ 0 & 0 & 0 & -\frac{1}{L_i} & 0 & -c_6 \end{bmatrix} \begin{bmatrix} z_1 \\ z_2 \\ z_3 \\ z_4 \\ z_5 \\ z_6 \end{bmatrix} \quad (61)$$

Therefore, it can be concluded that the closed-loop system is capable of achieving asymptotic stability.

IV. SIMULATION RESULTS AND DISCUSSION

The PV system, equipped with the proposed controller described in Figure 3, received a comprehensive examination under two distinct scenarios to ascertain its functionality. Firstly, the system was evaluated under various levels of solar irradiation while maintaining a constant temperature of 25° C. Secondly, the system was tested at different temperatures while keeping the irradiance constant at 1,000 W/m². The parameters for the studied system are provided in Table III, while Table IV details the controller parameters. These controller parameters were determined using a "trial-and-error" approach to ensure their effectiveness for the system's operation.

A. Controller Performances under Varying Irradiance with Constant Temperature of 25° C

The intensity of solar irradiation fluctuates throughout the course of a day, thereby influencing the MPP of the PVG, as shown in Table II. In order to evaluate the performance of the controller in the context of these varying conditions, the system was subjected to testing using the solar irradiation profile presented in Figure 4. The simulation commences with an irradiation level of 400 W/m², subsequently increasing to 800 W/m², then to 1,000 W/m², and finally decreasing back to 800 W/m².

TABLE III. PARAMETERS OF PV SYSTEM

Parameter	Symbol	Value
Grid voltage/frequency	e_g/F	220 V/50 Hz
VSI side Inductor	L_i	1.2 mH
Grid side Inductor	L_g	1.2 mH
Resistance of Inductor L_f/L_g	R_i/R_g	0.2/0.2 Ω
Filter Capacitor	C	6 µF
DC-link capacitor	C_{pv}	3.300 mF
Switching frequency	F_s	5 kHz

TABLE IV. NUMERICAL VALUES OF CONTROL PARAMETERS

Parameter	Value
c_1, c_2	1×10^8
c_3, c_4, c_5, c_6	1×10^4

Despite these fluctuations, the PV power rapidly reached its peak values of 38.515 kW, 79.395 kW, 99.608 kW, and 79.395 kW, respectively, within milliseconds, as portrayed in Figure 5. Figure 6 demonstrates that the grid current and voltage are in phase, thereby confirming that the unity power factor objective has been attained.

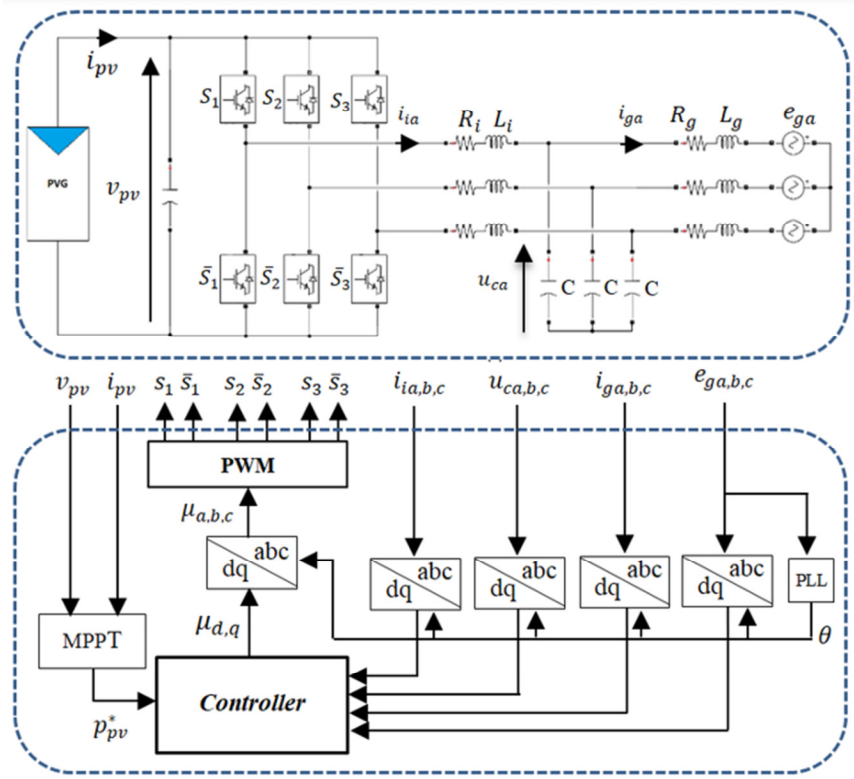

Fig. 3. Block diagram of the control system.

Furthermore, Figure 7 presents the harmonic components of the grid current at an irradiance level of 1,000 W/m², with a total harmonic distortion of approximately 0.12%. This evidence substantiates the efficacy of the LCL filter in reducing harmonic distortion.

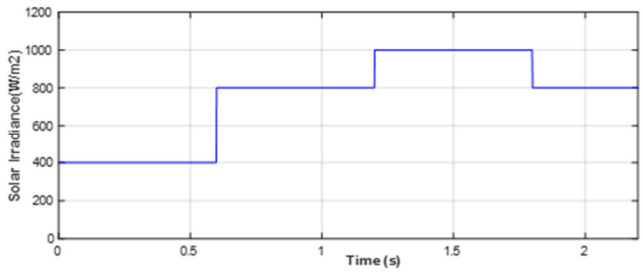

Fig. 4. Irradiance variation profile.

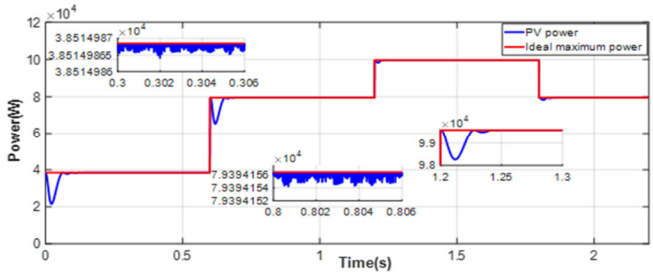

Fig. 5. PV power generated by the PVG compared to the ideal maximum power.

B. Controller Performances under Variable Temperature with Constant Irradiance of 1,000 W/m²

In this test case, the performance of the controller was examined under variable temperature conditions with a constant solar irradiance of 1,000 W/m². The simulation started at a temperature of 15° C, then increased to 25° C, followed by 35° C, and finally decreased to 25° C, as depicted in Figure 8. Despite these rapid temperature fluctuations, the PV power quickly reached its maximum values of 104.279 kW, 99.608 kW, 94.954 kW, and 99.608 kW, respectively, within a few milliseconds, as illustrated in Figure 9. Figure 10 shows the grid's voltage and current. Despite significant temperature fluctuations, the current remained sinusoidal and in phase with the voltage, confirming that the PFC objective was fully achieved. Furthermore, Figure 11 presents the FFT analysis of the grid current at 35°C, exhibiting a remarkably low THD of 0.12%. This THD value aligns with the requirements set forth by the IEEE-519 standard.

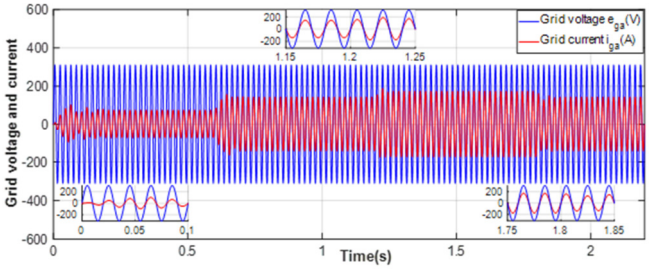

Fig. 6. Grid voltage and current signals (UPF verification).

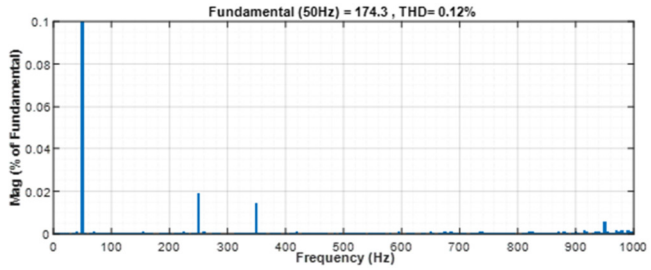

Fig. 7. Harmonics components of the grid current at an irradiance of 1,000 W/m².

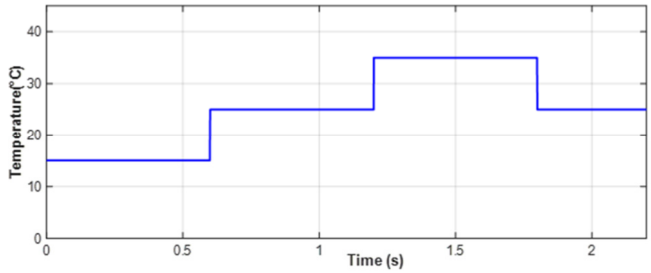

Fig. 8. Temperature variation profile

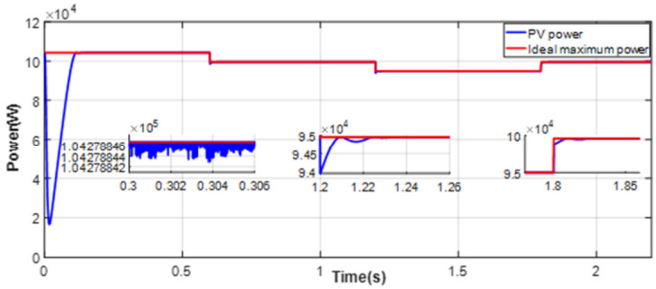

Fig. 9. PV power generated by the PVG compared to the ideal maximum power.

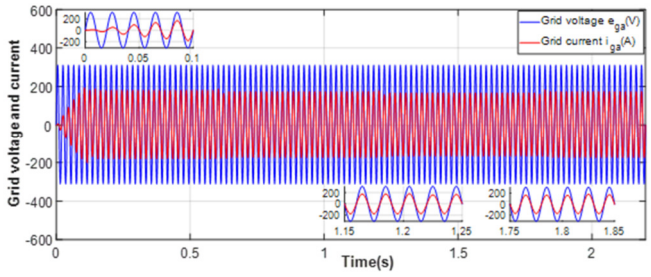

Fig. 10. Grid voltage and current signals (UPF verification).

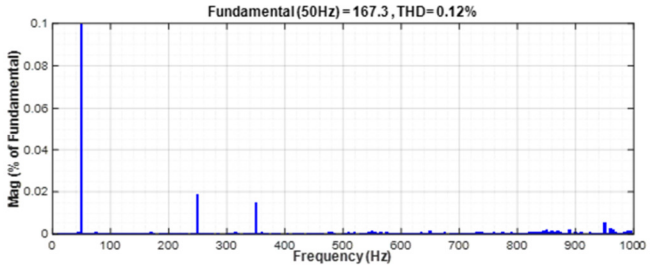

Fig. 11. Harmonics components of the grid current at a Temperature of 35°C.

V. CONCLUSIONS

This study presents a comprehensive mathematical model in the synchronous dq-frame for a Three-Phase Single-Stage Grid-Tied Photovoltaic System (TPSS-GTPS) with an LCL filter. The model is used to design a nonlinear backstepping controller with three primary objectives: ensuring a Unity Power Factor (UPF) on the grid side, optimizing the Photovoltaic (PV) system's performance to operate at its Maximum Power Point (MPP) under varying atmospheric conditions, and ensuring the asymptotic stability of the closed-loop system. The overall asymptotic stability of the system is demonstrated with mathematical precision through the application of Lyapunov techniques. The proposed control strategy has been subjected to extensive testing, which has demonstrated that it significantly enhances the quality of the power delivered to the grid in terms of tracking performance, system stability, and dynamics. Moreover, the incorporation of the LCL filter has been shown to result in a notable reduction in the Total Harmonic Distortion (THD) of the grid current.

REFERENCES

[1] Y. Chaibi, A. Allouhi, M. Salhi, and A. El-jouni, "Annual performance analysis of different maximum power point tracking techniques used in photovoltaic systems," *Protection and Control of Modern Power Systems*, vol. 4, no. 1, Aug. 2019, Art. no. 15, https://doi.org/10.1186/s41601-019-0129-1.

[2] S. Hota, M. K. Sahu, and J. M. R. Malla, "A Standalone PV System with a Hybrid P&O MPPT Optimization Technique," *Engineering, Technology & Applied Science Research*, vol. 7, no. 6, pp. 2109–2112, Dec. 2017, https://doi.org/10.48084/etasr.1374.

[3] L. W. Chong, Y. W. Wong, R. K. Rajkumar, and D. Isa, "An optimal control strategy for standalone PV system with Battery-Supercapacitor Hybrid Energy Storage System," *Journal of Power Sources*, vol. 331, pp. 553–565, Nov. 2016, https://doi.org/10.1016/j.jpowsour.2016.09.061.

[4] D. Xu, G. Wang, W. Yan, and X. Yan, "A novel adaptive command-filtered backstepping sliding mode control for PV grid-connected system with energy storage," *Solar Energy*, vol. 178, pp. 222–230, Jan. 2019, https://doi.org/10.1016/j.solener.2018.12.033.

[5] T. K. Roy and M. A. Mahmud, "Active power control of three-phase grid-connected solar PV systems using a robust nonlinear adaptive backstepping approach," *Solar Energy*, vol. 153, pp. 64–76, Sep. 2017, https://doi.org/10.1016/j.solener.2017.04.044.

[6] S. Kouro, J. I. Leon, D. Vinnikov, and L. G. Franquelo, "Grid-Connected Photovoltaic Systems: An Overview of Recent Research and Emerging PV Converter Technology," *IEEE Industrial Electronics Magazine*, vol. 9, no. 1, pp. 47–61, Mar. 2015, https://doi.org/10.1109/MIE.2014.2376976.

[7] H. Özbay, S. Öncü, and M. Kesler, "SMC-DPC based active and reactive power control of grid-tied three phase inverter for PV systems," *International Journal of Hydrogen Energy*, vol. 42, no. 28, pp. 17713–17722, Jul. 2017, https://doi.org/10.1016/j.ijhydene.2017.04.020.

[8] F. Z. Kebbab, L. Sabah, and H. Nouri, "A Comparative Analysis of MPPT Techniques for Grid Connected PVs," *Engineering, Technology & Applied Science Research*, vol. 12, no. 2, pp. 8228–8235, Apr. 2022, https://doi.org/10.48084/etasr.4704.

[9] K. Behih and H. Attoui, "Backstepping Terminal Sliding Mode MPPT Controller for Photovoltaic Systems," *Engineering, Technology & Applied Science Research*, vol. 11, no. 2, pp. 7060–7067, Apr. 2021, https://doi.org/10.48084/etasr.4101.

[10] M. A. G. de Brito, L. Galotto, L. P. Sampaio, G. de A. e Melo, and C. A. Canesin, "Evaluation of the Main MPPT Techniques for Photovoltaic Applications," *IEEE Transactions on Industrial Electronics*, vol. 60, no. 3, pp. 1156–1167, Mar. 2013, https://doi.org/10.1109/TIE.2012.2198036.

[11] M. A. Eltawil and Z. Zhao, "MPPT techniques for photovoltaic applications," *Renewable and Sustainable Energy Reviews*, vol. 25, pp. 793–813, Sep. 2013, https://doi.org/10.1016/j.rser.2013.05.022.

[12] J. Ramos-Hernanz, J. M. Lopez-Guede, O. Barambones, E. Zulueta, and U. Fernandez-Gamiz, "Novel control algorithm for MPPT with Boost converters in photovoltaic systems," *International Journal of Hydrogen Energy*, vol. 42, no. 28, pp. 17831–17855, Jul. 2017, https://doi.org/10.1016/j.ijhydene.2017.02.028.

[13] J. J. Nedumgatt, K. B. Jayakrishnan, S. Umashankar, D. Vijayakumar, and D. P. Kothari, "Perturb and observe MPPT algorithm for solar PV systems-modeling and simulation," in *2011 Annual IEEE India Conference*, Hyderabad, India, Dec. 2011, pp. 1–6, https://doi.org/10.1109/INDCON.2011.6139513.

[14] M. Aourir, A. Abouloifa, I. Lachkar, C. Aouadi, F. Giri, and J. M. Guerrero, "Nonlinear control and stability analysis of single stage grid-connected photovoltaic systems," *International Journal of Electrical Power & Energy Systems*, vol. 115, Feb. 2020, Art. no. 105439, https://doi.org/10.1016/j.ijepes.2019.105439.

[15] M. Boukhalfa, A. Benaissa, M. R. Bengourina, A. Khoudiri, and M. Boudiaf, "Performance Enhancement of the DPC Control Based on a VGPI Controller Applied to a Grid Connected PV System," *Engineering, Technology & Applied Science Research*, vol. 12, no. 2, pp. 8253–8258, Apr. 2022, https://doi.org/10.48084/etasr.4697.

[16] N. Altin, S. Ozdemir, H. Komurcugil, I. Sefa, and S. Biricik, "Two-stage grid-connected inverter for PV systems," in *2018 IEEE 12th International Conference on Compatibility, Power Electronics and Power Engineering (CPE-POWERENG 2018)*, Doha, Qatar, Apr. 2018, pp. 1–6, https://doi.org/10.1109/CPE.2018.8372540.

[17] P. R. Rivera, M. L. McIntyre, M. Mohebbi, and J. Latham, "Single — Stage three — Phase grid — Connected photovoltaic system with maximum power tracking and active and reactive power control based on nonlinear control," in *2017 IEEE Energy Conversion Congress and Exposition (ECCE)*, Cincinnati, OH, USA, Oct. 2017, pp. 1–7, https://doi.org/10.1109/ECCE.2017.8095753.

[18] A. Yahya, H. El Fadil, F. Giri, and H. Erguig, "Advanced control of three-phase grid connected PV generator," in *2014 International Renewable and Sustainable Energy Conference (IRSEC)*, Ouarzazate, Morocco, Oct. 2014, pp. 753–758, https://doi.org/10.1109/IRSEC.2014.7059763.

[19] M. Dursun and M. K. Dosoglu, "LCL Filter Design for Grid Connected Three-Phase Inverter," in *2018 2nd International Symposium on Multidisciplinary Studies and Innovative Technologies (ISMSIT)*, Ankara, Turkey, Oct. 2018, pp. 1–4, https://doi.org/10.1109/ISMSIT.2018.8567054.

[20] C. Poongothai and K. Vasudevan, "Design of LCL Filter for Grid-Interfaced PV System Based on Cost Minimization," *IEEE Transactions on Industry Applications*, vol. 55, no. 1, pp. 584–592, Jan. 2019, https://doi.org/10.1109/TIA.2018.2865723.

[21] C. Gurrola-Corral, J. Segundo, M. Esparza, and R. Cruz, "Optimal *LCL*-filter design method for grid-connected renewable energy sources," *International Journal of Electrical Power & Energy Systems*, vol. 120, Sep. 2020, Art. no. 105998, https://doi.org/10.1016/j.ijepes.2020.105998.

[22] M. B. Saïd-Romdhane, M. W. Naouar, I. Slama. Belkhodja, and E. Monmasson, "Simple and systematic *LCL* filter design for three-phase grid-connected power converters," *Mathematics and Computers in Simulation*, vol. 130, pp. 181–193, Dec. 2016, https://doi.org/10.1016/j.matcom.2015.09.011.

[23] W. Yin and Y. Ma, "Research on three-phase PV grid-connected inverter based on LCL filter," in *2013 IEEE 8th Conference on Industrial Electronics and Applications (ICIEA)*, Melbourne, VIC, Australia, Jun. 2013, pp. 1279–1283, https://doi.org/10.1109/ICIEA.2013.6566564.

[24] Y. Chen and F. Liu, "Design and Control for Three-Phase Grid-Connected Photovoltaic Inverter with LCL Filter," in *2009 IEEE Circuits and Systems International Conference on Testing and Diagnosis*, Chengdu, China, Apr. 2009, pp. 1–4, https://doi.org/10.1109/CAS-ICTD.2009.4960797.

[25] F. Liu, S. Duan, P. Xu, G. Chen, and F. Liu, "Design and Control of Three-Phase PV Grid Connected Converter with LCL Filter," in *IECON 2007 - 33rd Annual Conference of the IEEE Industrial Electronics Society*, Taipei, Taiwan, Nov. 2007, pp. 1656–1661, https://doi.org/10.1109/IECON.2007.4459978.

[26] X. Bao, F. Zhuo, Y. Tian, and P. Tan, "Simplified Feedback Linearization Control of Three-Phase Photovoltaic Inverter With an LCL Filter," *IEEE Transactions on Power Electronics*, vol. 28, no. 6, pp. 2739–2752, Jun. 2013, https://doi.org/10.1109/TPEL.2012.2225076.

[27] W. Hong, G. Tao, and H. Wang, "Adaptive Control Techniques for Three-Phase Grid-Connected Photovoltaic Inverters," in *Solar Photovoltaic Power Plants: Advanced Control and Optimization Techniques*, R.-E. Precup, T. Kamal, and S. Zulqadar Hassan, Eds. Singapore: Springer, 2019, pp. 1–24.

[28] W. Hong, G. Tao, and H. Wang, "An Output Feedback MRAC Scheme for Three-phase Grid-Connected Inverters in Photovoltaic Power Generation Systems," in *2018 IEEE Conference on Decision and Control (CDC)*, Miami, FL, USA, Dec. 2018, pp. 3439–3444, https://doi.org/10.1109/CDC.2018.8619111.

[29] P. T. Krein, J. Bentsman, R. M. Bass, and B. L. Lesieutre, "On the use of averaging for the analysis of power electronic systems," *IEEE Transactions on Power Electronics*, vol. 5, no. 2, pp. 182–190, Apr. 1990, https://doi.org/10.1109/63.53155.

[30] C. J. O'Rourke, M. M. Qasim, M. R. Overlin, and J. L. Kirtley, "A Geometric Interpretation of Reference Frames and Transformations: dq0, Clarke, and Park," *IEEE Transactions on Energy Conversion*, vol. 34, no. 4, pp. 2070–2083, Dec. 2019, https://doi.org/10.1109/TEC.2019.2941175.